AN EXPERIMENTAL AND NUMERICAL STUDY OF 3-D ROTOR WAKES IN HOVERING FLIGHT*

ICAS-82-4.4.3

M. NSI MBA, D. FAVIER, C. MARESCA

Institut de Mécanique des Fluides, LA03 du C.N.R.S.
1, rue Honnorat, 13003 Marseille, France

Abstract

Results of comparison between experimental and numerical studies on the 3-D wake of a hovering rotor are presented. The wind-tunnel investigation is conducted by means of X-hot wires and laser Doppler anemometry procedures to measure the 3-D velocity field under the rotor and to determine the tip vortex paths for several rotor configurations. Additional flow visualizations and rotor airloads coefficients are also carried out. The prediction model is based on the classical vortex theory with an empirically prescribed geometry of the wake. From the blade circulation distribution the rotor wake is represented by vortex lines which are allowed to freely adapt until a converged wake geometry is obtained. Then a new estimate of the blade circulation repartition can be deduced. The procedure is repeated, iterating until the compatibility between the adapted wake geometry and the blade circulation repartition is obtained. The validity range of the calculation model is deduced from comparison with experimental data obtained on instantaneous velocities and tip vortex paths, for different rotor parameters including solidy, number of blades, pitch angle, blade twist, and tip shape.

Nomenclature

a_o : Coning angle (deg)

b : Number of blades

c : Blade section chord (0.05 m)

C : Rotor torque

C_Q : Rotor torque coefficient ($C/\rho\pi R^3 V_e^2$)

C_T : Rotor thrust coefficient ($T/\rho\pi R^2 V_e^2$)

C_Z : Blade section lift coefficient

C_{ZM} : Mean rotor thrust coefficient ($6 C_T/\sigma$)

F.M : Figure of merit ($T^{3/2}/C\Omega (2\rho\pi R^2)^{1/2}$)

OXYZ : Rectangular coordinates system

r : Radial distance from axis of rotation

r_t : Vortex core radius

R : Rotor radius (0.750 m)

t : Time (sec)

T : Rotor thrust

U,V,W : Radial, tangential and axial velocities

V_e : Rotor tip velocity (ΩR)

$\bar{Z}$: Reduced thrust ($200 C_T/\sigma$)

σ : Rotor solidity ($bc/\pi R$)

$\theta_{0.75}$: Collective pitch angle at r = 0.75 R

θ_V : Blade twist angle (deg)

ψ : Blade azimuth or rotation phase (Ωt)

Ω : Rotor angular velocity (rad/sec)

ρ : Air density

Γ : Local blade circulation.

I. Introduction

During the course of the two last decades, the challenging problem of accurately predicting the rotor performances has given rise to extensive theoretical investigations. Many of these efforts have concerned the specific case of the hovering flight since it represents a simplified but necessary step for a better understanding of the more complex forward flight. When restricting to the hovering flight case, most of the developed prediction methods are based on a suitable modelling of the rotor wake geometry, and specially on the accurate determination of the vortex paths generated by the tip blades which constitutes an important factor for the calculation method.

A first generation of these methods have been built on rigid wake geometry prescribed either by theoretical considerations or by empirical formulas deduced from numerous experiments conducted on different rotor configurations. The works of Landgrebe[1] and those reported in reference (2) (see Cheney et al, Gray et al), give a wide survey of the state of the art concerning this kind of approach.

In recent years, a second generation of calculation model initiated by Kocurek et al[3], Scully[4], Gohard[5], Summa et al[6] in U.S., and by Courjaret et al[7], Pouradier et al[8] in France, introduces the concept of a free wake analysis. The basic change is that the wake model is allowed to freely distort owing to the downwash velocity distribution induced by the interaction between the tip vortex and the inboard vortex sheet. This adaptation wake geometry leads to a better prediction of the aerodynamic performances, and consequently to a more refined solution for airloads optimization of real rotors.

The present calculation model developed[9] at the Aerospatiale Helicopter Division belongs to the second generation, and has been already checked by comparison with experimental configurations. In the same view, and in order to check more completely the validity range of the operating code, a comprehensive test programme inclu-

*This work was supported by the "Direction des Recherches Etudes et Techniques" under Grant n°78/456.

ding a wide variety of rotor parameters has been undertaken at the I.M.F.M. with the support of the "Direction des Recherches Etudes et Techniques". The aim of this test programme is to establish the validity range of the code as function of various main rotor parameters, such as : number of blades, collective pitch angle, blade twist (linear and non linear), planform and tip shape. The influence of only some of previous parameters on the agreement between experiments and numerical results will be presented in this paper. In the light of these comparisons, limitations and future eventual changes in the predicting code will be considered too.

In the following sections, the calculation diagram for the induced velocities and the restrictions due to the code basic assumptions are firstly discussed. The test programme and associated experimental procedures are described in Section III. It can be already noticed that several unsteady measuring techniques will be required for the rotor wake survey : crossed hot wires and laser Doppler anemometries for measurements of instantaneous velocity field and tip vortex path ; flow visualizations for additional determination of the tip vortex path in a region very close to the rotating plane (where anemometry technique becomes inadequate), and also for the vortex core growing as function of the blade azimuth. Comparisons between experimental and numerical results are presented in the last section, and some eventual modifications of the calculation model are discussed for some specific rotor configurations.

II. Calculation model

The resolution technique and the basic theoretical equations used for the Aerospatiale computer code are described in details in references (7) and (8). Only summarized here are the main operations accomplished by the calculation diagram.

The rotor blade is considered as a lifting line spanning the quarter chord sections, and the bound vorticity is continuously distributed along this line. The wake is formed by a finite number of discrete vortex lines shed from each blade. The operation mode consists of dividing this wake in a strong rolled-up tip vortex filament as a result of grouping some tip vortices, and in several weaker trailing vortices lines representing the inboard vortex sheet. From this wake representation where the geometry of the inboard sheet is initially prescribed, the distorsion of the tip vortex line can be deduced from the downwash velocity distribution induced by the trailing and bound vortices.

The tip vortex line can be computed andadapted from its starting point ($\psi = 0$) on the emitting blade until the first encounter of the following blade which corresponds to the azimuth $\psi = 2\pi/b$. During the blade rotation concerning the azimuths $2\pi/b < \psi < 8\pi/b$, the tip vortex line is assumed to be convected and contracted according to the empirical laws synthesized in references (1) and (10). For $\psi > 8\pi/b$, the whole wake is replaced by a strong vortex ring of radius 1.2R, and located at the axial distance Z corresponding to $\psi = 8\pi/b$. The intensity of this fictive ring is assumed to represent four times the initial vorticity of the tip vortex line at its emitting point.

The input data required to start the calculation process are : the geometrical rotor configuration (solidity, collective pitch, blade twist, angular velocity, ...), the steady airloads and moment coefficients of the different airfoil sections, and the rotor thrust coefficient. From these given input data the wake geometry adaptation is obtained by the three-steps iterating procedure described in Figure 1.

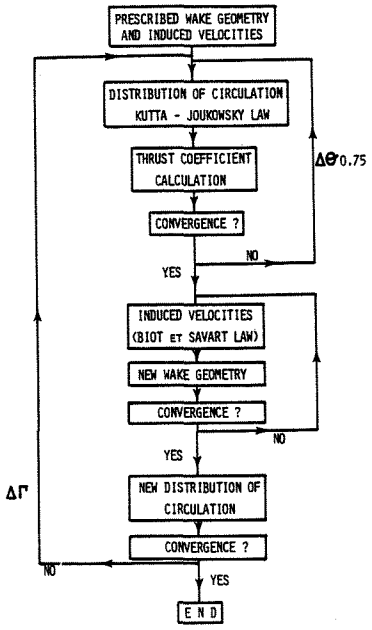

Fig. 1. Calculation block diagram

The three steps of the wake adaptation

1. The initial wake configuration represented by the tip vortex line and the inboard vortex sheet is prescribed as function of the input data of thrust coefficient and blade twist by application of the empirical formulas of contraction and convection along radius r and Z-axis. These laws obtained by Landgrebe[1] and Kocurek and Tangler[10], allow to specify the basic contraction and convection of both the sheet and the tip vortex, as functions of r/R, Z/R coordinates and of the azimuthal blade position ψ.

The bound circulation on the blade is estimated by a law of cosinus coefficients series deduced from 2-D aerodynamic airloads coefficients data, by means of Kutta-Joukowsky law. The vorticity shed behind each blade in the vortex sheet can be deduced from the previous blade circulation distribution. By applying the Biot and Savart law, the velocities induced by the vortex segments sheet in each point of the tip vortex line are then calculated.

2. A new wake configuration is obtained by integrating these induced velocities over small increment in time, corresponding to a small fraction $\Delta\psi$ of azimuthal rotation.

Steps 1 and 2 are repeated until in each of its points, the tip vortex line is tangent to the induced velocity calculated on these points. The so obtained wake configuration is called the freely wake geometry adapted to the developed velocity distribution.

3. The previous wake geometry adaptation leads to the determination of new incident velocities on the airfoil sections, and consequently by application of Kutta-Joukowsky law to a new estimation of the blade bound circulation repartition which is compatible with the calculated wake.

The process from steps 1 through 3 is repeated, iterating until the bound circulation of step 3 converges to the blade circulation distribution of step 1. As shown by the first loop of the calculation diagram (Figure 1), each iterative step on the $\Delta\Gamma$ circulation distribution implies a collective pitch angle change of an increment $\Delta\theta_{0.75}$ in order to keep constant the rotor trust coefficient C_T specified in the input data.

As the primary objective of the test programme is to directly check the validity range of the code on a variety of rotor configurations and parameters as large as possible, the previous calculation code operates in almost the same way as the one described in references(7) and (8) without any major changes. However, owing to the restrictive nature of some basic assumptions introduced in this model the limitations of the present operating mode are discussed below.

Operating mode limitations

First of all the partial geometric adaptation of the tip vortex line by the induced velocities effect is only accomplished on a fraction of revolution, for ψ varying from the initial emission at $\psi = 0$ to the first encounter ($\psi = 2\pi/b$). For $2\pi/b < \psi < 8\pi/b$ the empirical laws(1),(10) of wake contraction and vortex convection are no more modified. Moreover the far wake configuration ($\psi \gtrsim 8\pi/b$) remains artificially modelled by a vortex ring of arbitrary intensity.

It can be also noticed that the growth of the tip vortex core is neglected. The assumption made in the model consists of keeping constant the vortex core radius r_t at 5×10^{-3} R all along the tip trajectory. As exemplified in Figure 2, the influence of the vortex core growing is significant and can be directly analysed from calculation code results.

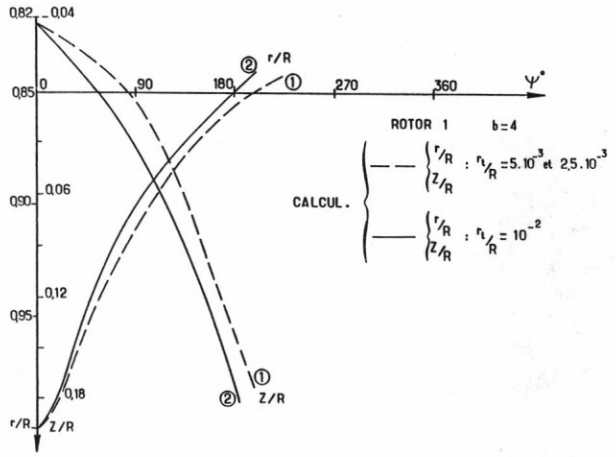

Fig. 2. Vortex core radius influence on calculated tip paths.

In this figure the calculated tip vortex path is represented by variations of the radial and axial coordinates (r,Z) where is located the vortex, as function of ψ. Three different core radius values of the tip vortex : $r_t/R = 2.5\times10^{-3}$, 5×10^{-3} and 10^{-2}, are considered in a four-bladed rotor configuration. For the two lower values, the results of calculation indicate the same merged tip path represented by a single dotted line on the Figure. As the core radius r_t is increased ($r_t/R = 10^{-2}$), the full lines show on the one hand that an increase of the wake contraction rate is observed along r/R, and on the other hand that the tip vortex is convected downstream with an increased velocity along the Z-axis.

Another point of limitation for the prediction method is that the blade beeing considered as a lifting line, the method cannot be applied to large evolutive tip shapes such as sharp swept tip or Ogee tip. In these cases, indetermined velocities appear at the discrete calculation points on the blade as shown by Kocurek in reference (3). Moreover the calculation procedure of induced velocities from numerical integration of Biot and Savart formula, is based on the Gauss method which introduces a finite number of calculation points along both the blade radius and the tip vortex line. A number of eleven Gauss points have been presently sufficient to ensure a converged process in the case of four-bladed rotors. However an optimization of this calculation points number must be considered to accelerate the convergence for two and three blades configurations.

III. Experimental conditions and procedures

The experimental investigation is conducted in the I.M.F.M.-S1 open circuit wind-tunnel of elliptical open test section (3.30x2.20 m^2). A photograph of the rotor set up is presented in Figure 3.

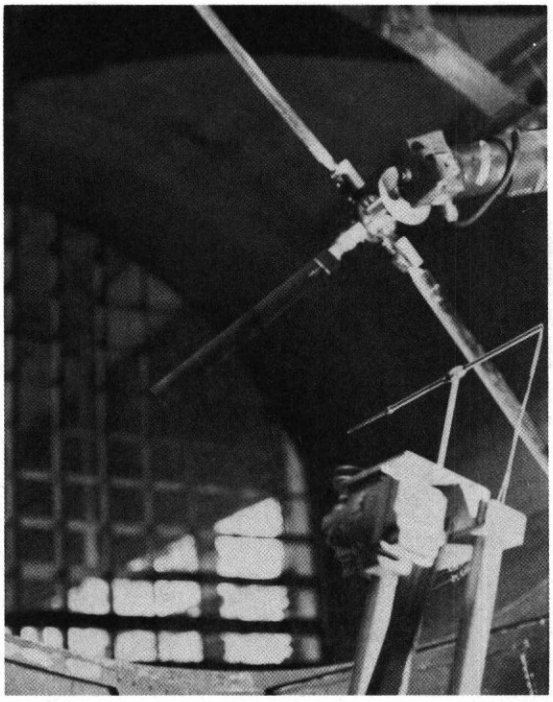

Fig.3. View of rotor and X-probe mounted on r,Z displacement device.

All the hovering tests presented in this paper are carried out with a constant rotor tip speed V_e of about 107 m/s. The model rotor (R = 0.750 m) used in the investigation has a hub (R_o = 0.104 m) fully articulated in flapping and lagging motions of the blades, and can be equiped with a number b = 2,3,4, or 6 blades. Each blade made of carbon fibres is of Aerospatiale manufactoring. Further details on the testing model can be found in reference (11).

The different sets of rotor configuration tested are numbered from 1 to 6 in Figure 4, and correspond to various combinations of blade twists, airfoil sections, and tip shapes. Two blade twist laws linear (Rotors 1,2,4,5,6) and non linear (Rotor 3) are tested with two different airfoil profiles (Boeing Vertol BV 23010, and O.N.E.R.A. OA209) of same chord length c = 0.05 m. Four tip shapes specified on Figure 4 are considered : a basic rectangular tip (Rotors 1,2,3), a swept tip (Rotor 4), a tapered tip (Rotor 5), and a parabolic tip (Rotor 6) which is actually tested in the wind-tunnel. All these different tip geometries are calculated so that the radii of the corresponding blades remain constant and equal to R=0.750 m.

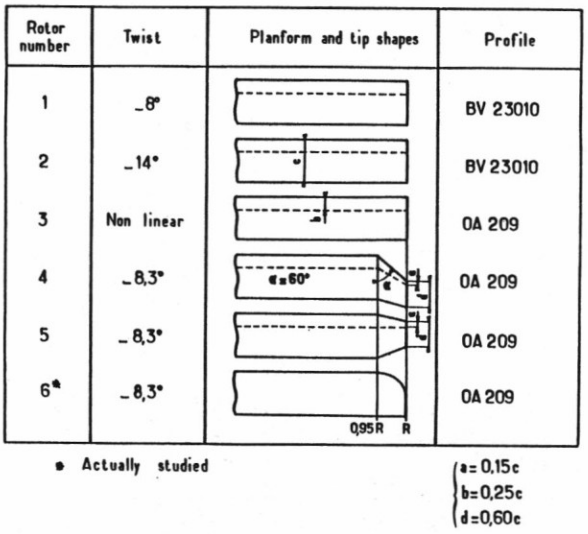

Fig. 4. Rotor, blades and tip shapes configurations

Rotor forces (thrust and torque) are measured with strain-gages bridges mounted on the supporting mast of the hub. Concerning wake measurements, several complementary techniques suited for unsteady flow analysis have been used for the rotor wake survey.

The induced velocities field is measured by an X-hot wires probe displaced behind the rotating plane along radial and axial coordinates (r,Z) by means of teledriven gears. The probe mounted on the (r,Z) displacement device can be seen on the photograph of Figure 3. The linearized output signals of the probe are digitized and stored by a 800 - channels data acquisition system, and then analysed within a computer (HP 9845). As function of time, the determination of the three velocity components radial tangential and axial (U,V,W), results from four recorded waveform signals deduced from two successive positions of the X-probe, which are obtained by rotating the probe of 90° around its symmetry axis. A more complete procedure of this measuring technique is given in reference (11).

The X-hot wires method can be properly used within the inboard wake until the radial distance corresponding to the tip vortex filament location is reached. Beyond this limit, the method becomes rapidly inadequate due to the presence of strong reversed flows in the wake of the hovering rotor. In these regions the laser Doppler anemometry technique has been used for velocities measurements.The L.D.A. bidimensional system operates in backscattering mode, and is provided with Bragg cells allowing the velocity measurement in the reversed flow regions. As for X-wires, in each point of the wake two bidimensional measurements deduced from two orthogonal positions of the fringes network are required for the complete 3-D determination of the velocity vector (see reference (11)).For each measurement point the fringes network can be moved along r and Z-directions by means of a 3-D displacement device linked with the whole optical system of light emission and reception. Moreover the front optical system is equiped with large focal lengths (1000 mm and 1800 mm) which permit a complete wide survey of the wake along r and Z coordinates. A view of the backscatter L.D.A. mounted on the displacement device can be seen on photograph of Figure 5.

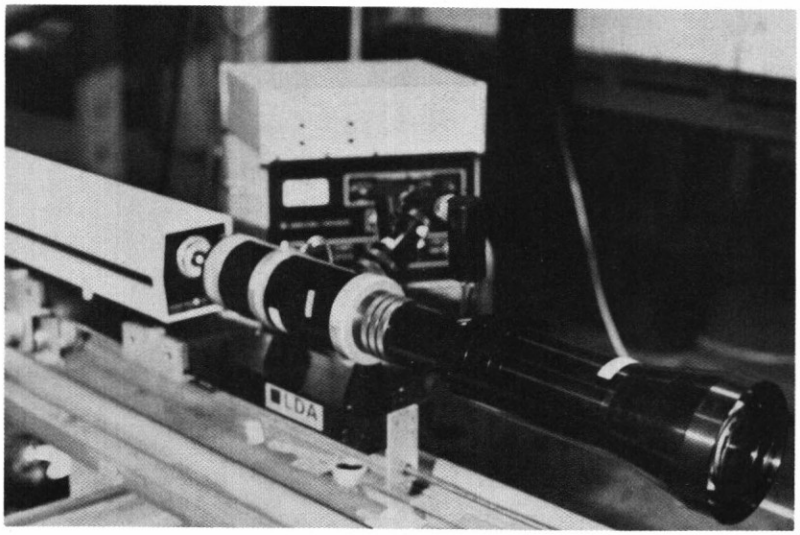

Fig. 5. View of Backscatter L.D.A.

The accurate determination of tip vortex lines has been carried out either by using the X-hot wires probe or by flow visualizations. Owing to the coning angle the X-probe can only be moved in a region of the near wake where collisions with the blades are precluded. Generally the safety conditions for the probe correspond to rotation azimuths higher than 40°.

Concerning the X-hot wires technique the tip vortex line determination is accomplished in the following mode: The probe is located in a given plane Z_V = cste of the near wake, and its output voltage is proportional to the axial velocity component W obtained as the sum of the X-branches voltages. This waveform W-signal is delivered on an oscilloscope whose scanning is synchronized with the blade rotation ($\psi = 0°$ corresponds to the blade passage over the probe location). In this plane (Z_V = cste) the probe is then gradually displaced along the blade radius direction from the hub towards the blade tip. During the displacement the vortex passage on the probe is detected by the occurence of both a W-velocity peak, and a sharp increase in turbulence level on the oscilloscope display. Since this vortex passage is detected at some (r_V, Z_V) position, the radial displacement is stopped and variations of the W-component as function of time are recorded for a complete period of rotation. The azimuthal phase lag $\Delta\psi_V$ between the vortex passage on the probe at ψ_V and the blade having shed the vortex at $\psi = 0°$, can then be determined from the time waveform of the axial velocity component. It can be noticed that using this procedure the tip vortex path is completely determined by the (r_V, Z_V, ψ_V) measurements so obtained.

In order to determine the tip vortex path for wake regions very close to the blade, a visualization flow technique has also been used. The procedure consists of continuously injecting white smoke filaments in the flow, by means of an emitting profiled rod which has been located in the outside reversed flow region just downstream the rotating plane. A stroboscopic flash synchronized with the blade rotation lights up the emission lines of smoke filaments which are filmed by a video camera system and recorded on a magnetoscope tape. From the unwind of the magnetic tape record, the emission lines are revealed on a monitor screen for any ψ of the rotation. When a specific ψ is selected on the frame, the magnetoscope can be stopped and photographs of the corresponding flow pattern taken on the screen.

As an example the photographs of Figure 6 show the flow patterns of two smoke emission lines visualized at $\psi \sim 0°$ and $\psi = 20°$ in the configuration of Rotor 1. These emission lines clearly reveal the intersection of the tip vortex trajectory with the diametral plane where the smoke filaments are emitted. From different photographs taken at several phases of the period it becomes easy to directly determine the tip vortex location in space and time, and so to complete the (r_V, Z_V, ψ_V) measurements obtained with the X-probe technique.

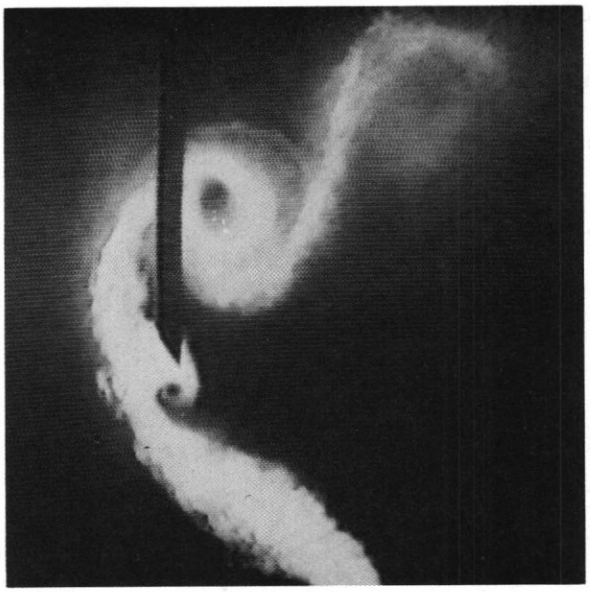

(a) $\psi \simeq 0°$

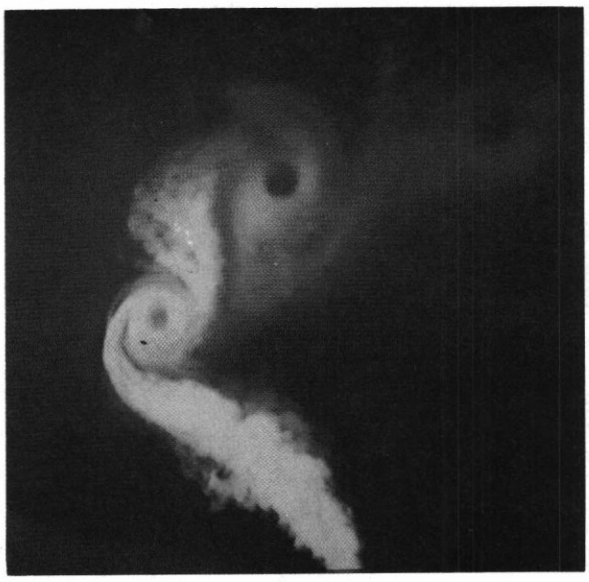

(b) $\psi = 20°$

Fig. 6. Tip vortices visualisations. Rotor 1

Moreover, by using the flow visualization technique previously described it has been possible to determine the core radius evolution of the tip vortex as function of phase, this last one being measured from the continuous magnetic tape record. Variations of the core radius r_t versus ψ so obtained by the visualization method, are presented in Figure 7 for several configurations (Rotors 1,3,4,5) with a constant collective pitch $\theta_{0.75} = 10°$. It can be noticed that during a relatively short fraction of the period, e.g. from the vortex shedding on the blade at $\psi = 0°$ until the phase where the first blade interaction takes place at $\psi = 90°$, the core radius undergoes a sharp growth since it can double its dimension.

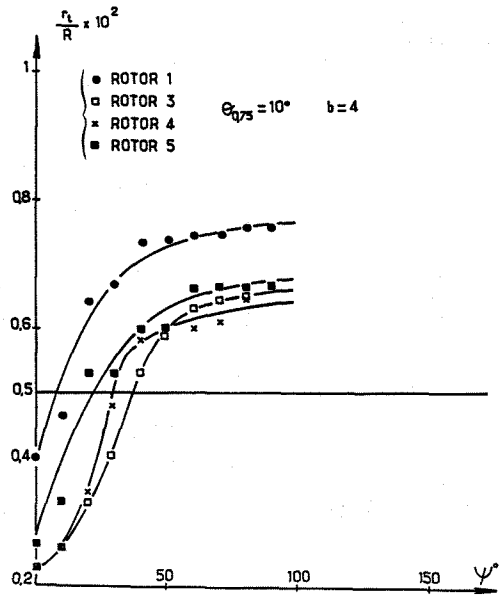

Fig. 7. Vortex core radius variation VS ψ

This results clearly demonstrates that the assumption of constant vortex core dimension for the calculation model (see Section II) must be improved, specially during the wake geometry adaptation step ($\psi < 45°$) where the vortex core growth is important as shown on figure 7.

The test programme conducted by using previous experimental techniques is summarized on the table of Figure 8. Results relative to the configuration of rotor 6 are not yet available. The rotor configurations numerically investigated are also specified in this table.

In Figure 8 The velocity measurements obtained by means of either the X-hot wire technique or the L.D.A. method, have been carried out for 2 or 3 downstream planes Z = cste. Their positions behind the rotating plane correspond to phases $\psi = 4\pi/3b$, $2\pi/b$, $3\pi/b$ of the rotation. In each of these planes the time dependent variations of velocity components have been recorded for 10 different radial positions. The increment between these radial positions becomes smaller in the vicinity of the tip vortex radial location.

IV. Comparisons between numerical and experimental results

The results presented in this section allow to check the calculation model on a variety of five different rotor configurations by direct comparison with experiments as indicated in Figure 8. In their respective range of variation (see Figures 4 and 8) it is then possible to analyse the influence of the following parameters : collective pitch $\theta_{0.75}$, number of blades b, blade twist, and tip shape. When the numerical results are available, the comparisons with experimental data are based and discussed on three aerodynamic characteristics of the rotor and its associated wake : the rotor performances characterized by the Figure of merit, the tip vortex paths, and the induced velocities in the wake.

Figures of merit

The experimental Figure of merit evolution is presented in Figure 9 versus the reduced thrust parameter $\bar{Z}$, for three rotor configurations (Rotors 1,4,5) with the same number of blades b = 4. The reduced thrust ($\bar{Z} = 200\ C_T/\sigma$) is varying within the range $10 < \bar{Z} < 20$ and corresponds to a mean thrust coefficient varying from 0.3 to 0.6 as indicated by the subscale abscissa on the Figure. For this evolution F.M. = F.M. ($\bar{Z}$) only deduced

$\theta_{0,75}$		10°							8°					6°	
b		4					2		4		3	2		4	2
Rotor number (see fig.4)		1	2	3	4	5	1	2	1	2	1	1	2	1	1
$\bar{Z}$		17,10	17,10	16,42	19,46	19,47	21,91	21,91	13,85	13,85	12,80	18,70	18,70	11,70	11,52
TIP VORTEX PATH	Experiments	FC V	FC V	FC V	FC V	FC V	FC	FC	FC	FC	FC	FC	FC	FC	FC
	Compar. calcul-exper.	+	+	−	Calcul no accurate	+	x	x	+	x	x	No convergence	x	−	No convergence
INDUCED VELOCITIES	Experiments	FC L	FC L	FC	FC	FC	FC L	FC	FC	FC	FC L	FC	FC	FC	FC
	Compar. calcul-exper.	+	+	−	Calcul no accurate	−	−	x	+	+	−		x	−	

FC : X Hot-wires ; L : Laser ; V : Visualization
+ : Good, x : Acceptable ; − : Bad

Fig. 8. Table test programme for different rotor configurations.

from experiments, the torque measurements are not available for rotors 2 and 3. However, it appears that since $\bar{Z} > 15$ the performances reached with the swept tips (Rotor 5) are better than the ones obtained with tapered tips (Rotor 4). An opposite behaviour relative to rotors 4 and 5 is observed for $\bar{Z} < 15$. For higher values of the reduced thrust parameter ($\bar{Z} > 20$) the linear twisted blades with rectangular tips (Rotor 1) are shown to present a better efficiency.

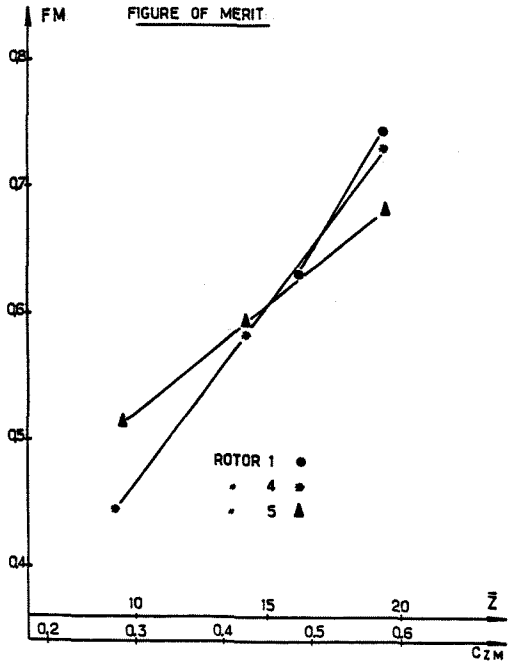

Fig. 9. Figures of merit VS, $\bar{Z}$ and C_{ZM}

The figure of merit behaviour observed on rotors 4 and 5 for $\bar{Z} < 15$, appears to be in good agreement with similar results presented in reference (12) and obtained with the same rotor configurations excepted the rotor tip speed which was equal to V_e = 196 m/s, representing about twice the present one (V_e = 107 m/s). The influence of velocity tip V_e can be considered as negligible on Figure of merit, at least when parameters $\bar{Z} < 16$ (or $C_{ZM} < 0.55$) are concerned. It can also be noticed that previous results of Figure 9 on F.M. obtained for the same number of blades b, require to be completed by additional future experiments which will be conducted at I.M.F.M. by varying the b parameter.

Concerning the comparison between calculated and measured Figures of merit, two examples are given on tables 1 and 2 for the four-bladed configurations of rotors 1 and 5.

Rotor 1	$\theta_{0.75}$	F.M.
Test	8.00	0.629
Predicted	8.61	0.649
Test	10.00	0.740
Predicted	11.05	0.705

Table 1 : Figures of merit calculated and measured for Rotor 1, b = 4

Rotor 5	$\theta_{0.75}$	F.M.
Test	8.00	0.596
Predicted	10.60	0.573
Test	10.00	0.683
Predicted	13.19	0.762

Table 2 : Figures of merit calculated and measured for Rotor 5, b = 4.

From these comparisons it appears that for all the rotor configurations considered, the predicted collective pitch angle $\theta_{0.75}$ always exceeds the experimental value. These over-estimations are of about 10 % for rotor 1 (table 1), and can reach 32 % for rotor 5 (table 2). However, the agreement between experiments and predictions is shown to be better on the Figure of merit when considering the results obtained on F.M. at fixed collective pitch. The relative error on F.M. values do not exceed 5 % on table 1, and 12 % on table 2.

Tip vortex paths

Results of calculation-experiment comparison on the tip vortex paths are summarized in the table of Figure 8 by indicating an agreement comment (good, acceptable, or bad), and allow to deduce some general trends.

For relatively high rotor solidity (b = 4) and high collective pitch angles ($\theta_{0.75} = 10°$), the agreement calculation - experiment appears to be good for all the rotor configurations tested (see Figure 8), except for the non linear twisted blades of Rotor 3 case which will be discussed later on. For smaller collective pitch angles (6°, 8°) only linear twisted blades with rectangular tips have been presently available for both experiments and predictions, and the agreement is shown to be bad for the lower value and acceptable for $\theta_{0.75} = 8°$.

To give some examples of the agreement appreciation mode given in figure 8 for the calculation - experiment comparison, four rotor configurations (Rotors 1,3,4,5) are more specifically analysed below for $\theta_{0.75} = 10°$ and b = 4.

Rotor 1

For this configuration the corresponding comparison on tip vortex path is shown on Figure 10. The predicted path represented by full lines appears to be in good agreement with experiments, specially for $0° < \psi < 150°$ representing the near

and middle wake. As $\psi > 150°$ experimental data gradually deviate from predictions, indicating a less good far wake modelling in the calculation code.

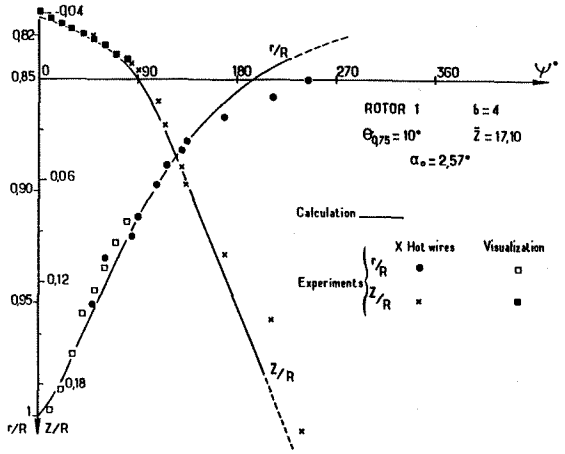

Fig. 10. Calculated and measured tip vortex paths Rotor 1.

It can be seen that the two experimental determinations of the tip vortex path by either X-probe or visualization method are in good agreement. For the wake region very close to the blade ($0.95 < r/R < 1$, $-0.04 < Z/R < -0.02$) the visualization results fairly extend the tip path deduced from X-probe survey.

Rotor 3

In this configuration the experimental results of Figure 11 indicate a bad comparison between X-probe and visualization data. When hovering tests were conducted on these non linear twisted blades, a characteristic instability in both space and time for the tip vortex line has been indeed observed.

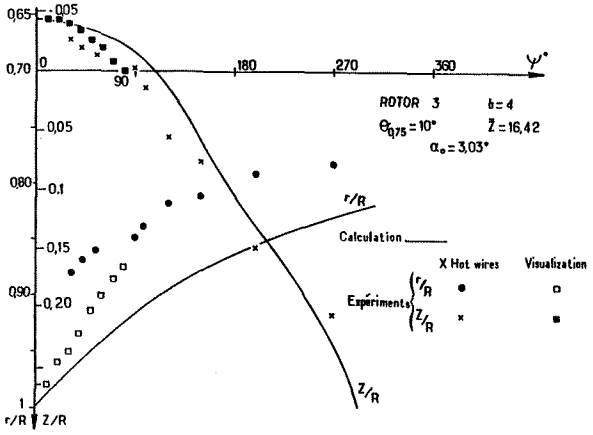

Fig. 11. Calculated and measured tip vortex paths . Rotor 3.

These instabilities brought some scattering on the determination of radial location and phase (r,ψ) of the tip vortex, and have required a 200 - cycles averaging procedure when recording the W - waveform velocity by X-hot wires. On the other hand, it was easy to select during the unwind of visualizations magnetic tape, the exact phase where the tip vortex was perfectly shape formed. This explains that the (r,Z,ψ) vortex determination by visualization procedure gives more regular and reliable data.

Concerning the comparison between calculation and experiment of Figure 11, a deviation is observed on the tip path evolutions and an improvment of calculation model is required for this rotor configuration. This improvment can be brought by including within the calculation code the growth of the vortex core radius during the first part of the period $0° < \psi < 90°$. Indeed for this rotor 3 configuration the experimental core radius evolution $r_t = r_t(\psi)$ presented on Figure 7 indicates, that when compared to the constant core radius value ($r_t/R \simeq 5 \times 10^{-3}$) used in the computer code, the real radius remains lower than this value for $\psi < 40°$, and then increases again and stabilizes at a higher value for $\psi \sim 80°$. By considering the predicted results on tip vortex path of Figure 2, it can be seen that the introduction of a smaller core radius ($r_t < 5 \times 10^{-3}$) in the calculation does not affect the result (see dotted lines). On the other hand, introducing a higher core radius (represented by full lines) will lead to a downward expansion of the Z/R-line and to an inner contraction of the r/R-line. Turning now on results of Figure 11, it can be concluded from the previous considerations that introducing the experimental core radius growth in the code will improve the calculation model. Specially for the region $\psi > 30°$ where the $dr_t/d\psi$ gradient variation becomes important.

Rotor 4

For this rotor configuration the predicted results were not available yet. However, the corresponding experimental data are given in Figure 12 in order to show the tip vortex trajectory for swept tips. A radial wake contraction along the r/R-line smaller than those obtained on rotors 1 and 3 (Figures 10 and 11) can be observed.

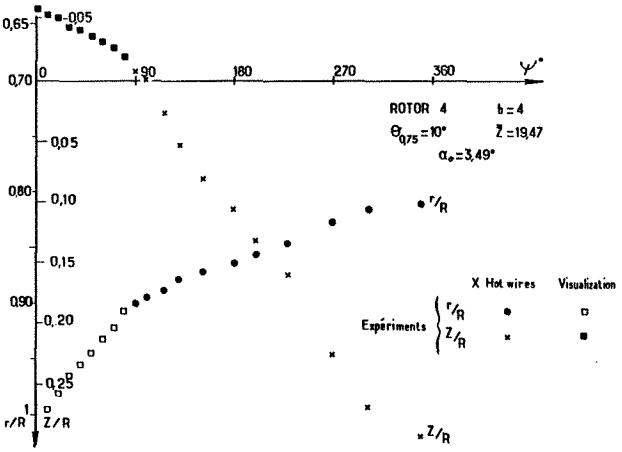

Fig. 12. Experimental tip vortex path . Rotor 4.

Rotor 5

Results of Figure 13 present the calculation - experiment comparison for the linear twisted blades with tapered tips. The good agreement obtained for $90° < \psi < 270°$ indicates that the far wake model-

ling seems to be adequate in this case. However, as for the rotor 3 previously discussed, the introduction of the vortex core growth for $0° < \psi < 90°$ will improve the predicted results in this region.

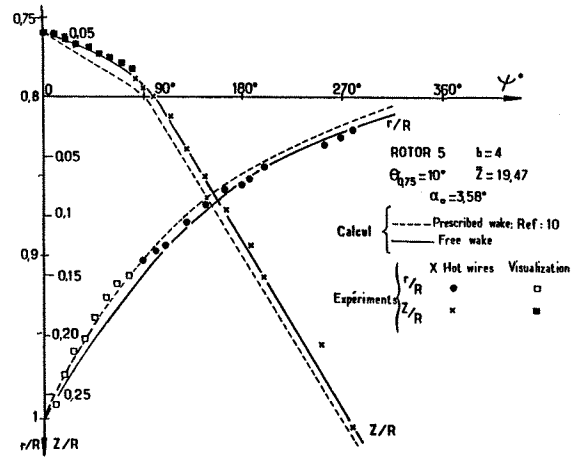

Fig. 13. Calculated and measured tip vortex paths Rotor 5.

In this figure are also represented the results obtained from the calculation model without the free wake analysis step discussed in Section II. In this case the tip vortex line and the inboard sheet evolutions are only given by the prescribed wake laws of reference (10), and are represented by dotted lines on the Figure. It can be observed along the r/R-line a better agreement on comparisons when the wake geometry adaptation is introduced within the prediction code (full lines).

Induced velocities in the wake

As for the previous tip vortex paths the agreement appreciations on comparison between measured and calculated induced velocities are incorporated in the table of Figure 8. When considering the agreement appreciations given for both the tip vortex lines and the induced velocities (two last table line blocks), it can be concluded that a good comparison agreement obtained on tip vortex paths do not imply a good one on induced velocities (see Rotor 5 for b = 4 and Rotor 1 for b = 3). This fact can be attributed to an inadequate far wake modelling (radius, Z-location, and intensity of the vortex ring) for some specific rotor configurations .

The vector velocity components U,V,W have been measured as function of time for different planes Z = cste behind the rotating plane and several stations along blade radius. For a proper comparison between calculation and experiments it seemed more instructive to present the results for a fixed plane Z = cste and a fixed azimuth ψ =cste, as function of the radial position r/R. Two examples of comparison on W-component at phases $\psi = 0°$ and $\psi = 60°$ are given in Figures 14 and 15, for the plane located at Z/R = 0.06 behind the rotor 1 with b = 4 and $\theta_{0.75} = 10°$.

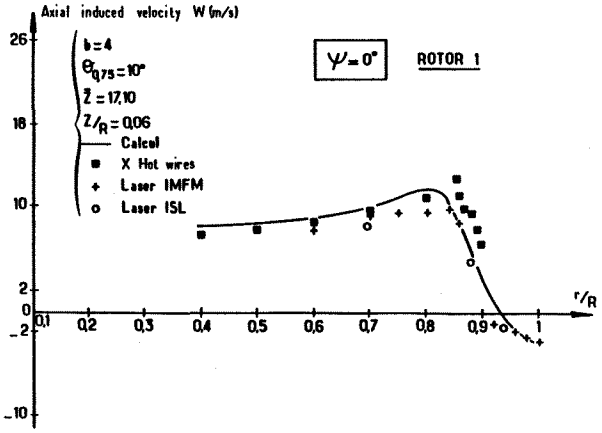

Fig. 14. Calculated and measured axial induced velocity VS r/R ; rotor 1 ; Z/R = 0.06 and $\psi = 0°$.

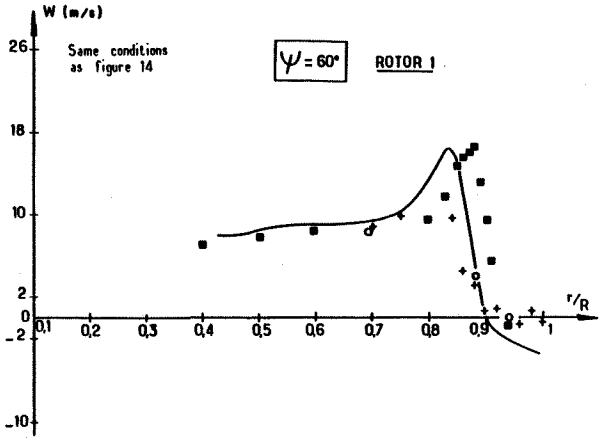

Fig. 15. Calculated and measured axial induced velocity VS r/R ; rotor 1 ; Z/R = 0.06 and $\psi = 60°$.

In these Figures the experimental W-component data are obtained as the result of three different measuring techniques : the X-hot wires method, and two L.D.A. measurement modes from I.S.L. and I.M.F.M. Laser System procedures. A good agreement is observed on the data obtained by these different measuring techniques, and the velocity level predicted by calculations also agrees with experiments. The slight difference observed in Figure 15 between the calculated and measured peaks of axial velocity, can be explained by the slight deviation between calculation and experiment already obtained in Figure 10 for the tip vortex paths comparison.

An additional example of comparison relative to rotor 5 (b = 4, $\theta_{0.75} = 10°$) is presented in Figure 16 for the axial component W at $\psi = 0°$.

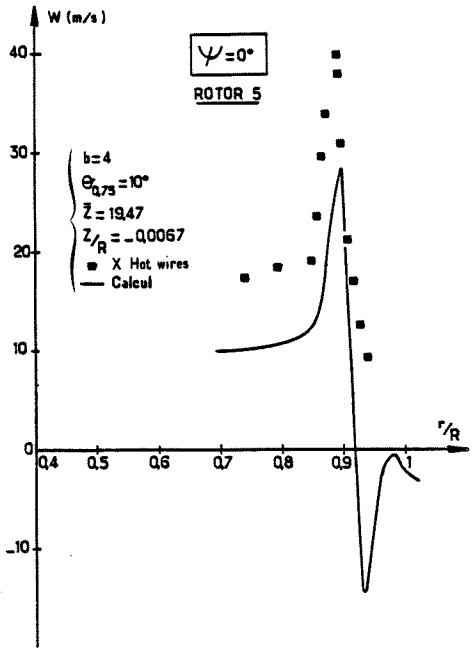

Fig. 16. Calculated and measured axial induced velocity VS r/R ; Rotor 5 ; Z/R=-0.007 and $\psi = 0°$.

For the downstream plane Z/R = - 0.0067 considered in this Figure, the tip vortex is located at $\psi = 0°$ (or $\psi = 90°$) and r/R = 0.89 as shown by results of Figure 13. The occurence of the axial velocity peak is well confirmed in Figure 16 by X-hot wires data and calculated results, which both indicated the tip vortex detection at radius $Z/R \sim 0.89$ for this phase $\psi = 0°$.

Comparisons previously presented in Figures 14,15,16, only concern the W axial induced velocity. From similar comparisons realised on tangential and radial velocities it can be concluded that the agreement appreciations given in the table test of Figure 8 remain also valid for the two other velocity components.

V. Conclusions

By direct comparison with experiments, a calculation model of rotor performances for the hovering flight case has been checked on induceed velocities in the wake and tip vortex paths. Although the variety of rotor configurations tested has been limited, the agreement between calculation and experiment has been checked for several rotor parameters such as : number of blades, collective pitch angle, linear and non linear blade twist, tip shape.

The calculation mode appears to be adequated to the partial wake geometry adaptation of tip vortex lines for azimuths varying from $\psi = 0$ to $\psi = 2\pi/b$, and for four-bladed rotors with relatively high collective pitch ($\theta_{0.75} = 10°$) and linear twisted blades. For non linear twisted blades, it has been shown that the agreement between calculation and experience could be improved by including within the calculation code the time dependant evolution of the tip vortex core. This evolution of the vortex core radius can be realised on the base of an empirical formula deduced from a wide variety of experiments carried out in a large range of rotor configurations.

It has also been shown that even when the near rotor wake is well calculated by the operating model, as it is the case for tapered tips blades, the corresponding induced velocities field may be inaccurately predicted owing to the lack of suited far wake modelling. Moreover, the comparisons between calculation and experiment realised for linear twisted blades with rectangular tips have also indicated that some improvments are required in the operating model, specially for low number of blades and small collective pitch angle rotor configurations.

At last, this calculation mode requires to be extended to larger evolutive shape tips such as swept tips, for which some new empirical modelling on tip vortex paths and tip vortex core evolutions could be deduced from the test programme conducted at I.M.F.M.

Acknowledgements

The authors are grateful to MM. J.M. POURADIER and A. VUILLET, Engineers at the Aerospatiale Helicopter Division, for their continued interest and useful discussions during the course of this study.

References

1. A.J. Landgrebe : "An analytical and experimental investigation of helicopter rotor hover performance and wake geometry characteristics", U.S.A. AMRDL Technical Report 71-24, June 1971.
2. "Aerodynamics of rotary wings", AGARD Conference n°111. Fluid Dynamics Panel Specialists"Meeting, Marseille, Sept. 1972.
3. J.D. Kocurek, L.F. Berkowitz, F.D. Harris : "Hover performance methodology at Bell helicopter Textron", A.H.S. Forum Proceedings, Washington D.C., May 1980.
4. M. Scully : "Computation of helicopter rotor wake geometry and its influence on rotor harmonic airloads", MIT ASRL TR 178-1, March 1975.
5. J.D. Gohard : "Free wake analysis of wind turbine aerodynamics", MIT ASRL TR 184-14, Sept. 1978.
6. J.M. Summa, D.R. Clark : "A lifting surface method for hover/climb airloads", A.H.S. Forum Proceedings, Washington D.C., May 1976.
7. R. Courjaret, A. Cassier : "Aérodynamique des rotor : calcul des performances au point fixe avec sillage expérimental figé", D.R.E.T., Grant n° 75/276, Lot N°1, 1976.
8. J.M. Pouradier, A. Bremont, J. Gallot : "Aérodynamique des rotors en vol stationnaire : mise en équilibre", D.R.E.T., Grant n° 75/276, Lot n° 2, 1978.
9. J.M. Pouradier, E. Horowitz : "Aerodynamic study of a hovering rotor", Proceedings of 6th European Rotorcraft and Powered lift Forum, Bristol, September 1980.
10. J.D. Kocurek, J.L. Tangler : "A prescribed wake lifting surface hover performance analysis", 32nd Annual Forum of the American Helicopter Society, May 1976.
11. M. Nsi Mba, D. Favier, C. Maresca, J. Rebont :

"Calcul et mesure du champ des vitesses induites par un rotor d'hélicoptère (vol stationnaire), D.R.E.T., Grant n° 78/456, December 1980.
12. J.P. Silvani, A. Vuillet : "Aerospatiale survey of wind tunnel testing of small and large scale rotors", Proceedings of 7th European Rotorcraft and Powered lift Aircraft Forum, Garmisch, September 1981.